

## High-frequency rheology of three adhesive polymers

Kira L. Eliasen, 1,a) Christian Brinkmann, 2,b) Sebastian Schmidt-Lehr, 2,c) Andreas Westphal, 2,d) Jeppe C. Dyre, 1,e) and Tina Hecksher 1,f)

<sup>1</sup>"Glass and Time," IMFUFA, Department of Science and Environment, Roskilde University, Universitetsvej 1, Roskilde 4000, Denmark <sup>2</sup>tesa SE, Hugo-Kirchberg-Straße 1, Norderstedt 22848, Germany

(Received 15 April 2025; final revision received 17 September 2025; published 13 October 2025)

#### **Abstract**

This paper reports linear shear-modulus rheological data for three adhesives. The data were obtained using a recently developed one-disk piezo-ceramic shear transducer that measures the complex shear modulus in a broad dynamical range, reaching frequencies up to 70 kHz [M. Mikkelsen et al., J. Rheol. 66, 983-1003 (2022)]. We first demonstrate consistency with data obtained by a standard rheometer. The paper proceeds to discuss new insights which the high-frequency data give rise to, with a focus on two questions important for applications: To which degree does time-temperature superposition apply? What is the temperature dependence of the high-frequency plateau shear modulus? For both questions, it is demonstrated that reliable predictions are much easier to arrive if high-frequency data are available. Thus, we show that the commonly used master-curve construction may lead to erroneous conclusions if based only on standard rheometer data. Finally, the data for the high-frequency plateau modulus are used to investigate the shoving-model prediction for the non-Arrhenius temperature dependence of the average relaxation time, which is found to apply to a reasonable approximation for all three samples. © 2025 Published under an exclusive license by Society of Rheology. https://doi.org/10.1122/8.0001034

#### I. INTRODUCTION

When it comes to characterizing the dynamic properties of materials, a fundamental quantity is the complex frequencydependent shear modulus,  $G^*(\omega)$  (in which  $\omega$  is the angular frequency) [1-8]. This quantity is also important for theory development [9–14]. Standard commercial rheometers for dynamical-mechanical analysis (DMA) are excellent for measuring  $G^*(\omega)$  at relatively low frequencies and low moduli, but the instrument resonance sets an upper limit of the frequency range to typically around 100 Hz. This is unfortunate because, depending on the material in question, there may well be relaxation processes in the kilohertz, megahertz, and even gigahertz regions [12,15]. Such processes are important for some material properties, for instance for predicting the shock-impact resistance of cars or mobile phones with glued components, for which the high-frequency shear-mechanical properties of the adhesive are crucial. Measuring mechanical properties of materials at high frequencies is notoriously difficult, however. Moreover, the instrument compliance of standard rheometers makes the measurement of hard materials challenging and the results less reliable than for softer materials.

10-70 kHz and down to millihertz is the piezoelectric shearmodulus gauge (PSG) consisting of three concentric piezoelectric ceramic (PZ) disks [26]. The PSG can be used at temperatures below roughly 200 °C (depending on the Curie temperature of the piezoelectric ceramic material) and is sensitive to moduli in the range from  $10^6$  to  $10^{10}$  Pa. Recently, a simplified version of the PSG consisting of a single PZ disk

close to their glass-transition temperature, solid samples that

Several different methods have been developed for measuring  $G^*(\omega)$  at frequencies higher than available through  $\vec{\sigma}$ 

commercial rheometers. Reviews by Willenbacher and §

Oelschlaeger [16] and more recently by Schroyen et al. [17]

cover techniques going up to 100 MHz, which employ

various modes of piezoelectric transducers (linear shear, tor- as

sional, compression, rotation) or use resonances modes to \( \frac{N}{2} \)

obtain discrete data points in the ultrasonic frequency range

[17]. Other specialized techniques use light-matter interaction

[18], e.g., for optical generation and detection of shear-

acoustic waves in liquids [19-21], for surface-wave detection

[22], or in dynamic light scattering in the multiple scattering

limit [23,24]. Methods based on piezoelectric transducers

like the one used below are also becoming popular [25].

Besides different frequency ranges, these techniques also

have different modulus sensitivities, operating temperatures,

strain ranges, and sample volume capacities. Hence not all

A mature method working in the acoustic region from

techniques are equally suited for specific sample types.

b)Electronic mail: Christian.Brinkmann@tesa.com was described [27] offering several advantages compared to c)Electronic mail: Sebastian.Schmidt-Lehr@tesa.com the three-disk version, in particular, extending the types of samples that can be investigated to include solid samples such as polymers. The PSG is well-suited for viscous liquids

a)Electronic mail: kira-eliasen@live.dk

d)Electronic mail: Andreas.Westphal@tesa.com e)Electronic mail: dyre@ruc.dk

f)Author to whom correspondence should be addressed; electronic mail: tihe@ruc.dk

<sup>© 2025</sup> Published under an exclusive license by Society of Rheology. J. Rheol. 69(6), 991–1003 November/December (2025)

can be melted to adhere to the surface of the PZ disk, and adhesive samples including samples undergoing curing; the method is less well-suited for samples that do not flow, e.g., rubbers, because they need to be glued to the PZ surface.

There are not many methods covering the region from the upper frequency limit of standard rheometers to the ultrasonic frequencies. Chen and Lakes [28] obtained a frequency and modulus range similar to that of the PSG by means of an electromagnetically driven torsional apparatus. This method is only suited for samples that are solid at room temperature, however. Verbaan *et al.* extended the upper limit of subresonant techniques by introducing a high-viscous damper into the design enabling the measurement of the viscoelastic properties of high-viscosity fluids ( $\eta > 100 \,\mathrm{Pa}\,\mathrm{s}$ ) in the frequency range between 10 Hz and 10 kHz. Koganezawa *et al.* [29] developed a shear setup working in the range from 300 Hz to 5 kHz for solid materials.

This paper compares data on three different solid polymer adhesive samples obtained by a standard rheometer to data of the new single-disk PSG setup. We demonstrate good agreement between the methods in the region of overlap. We show that the commonly used master-curve construction may lead to erroneous conclusions if based only on standard rheometer data. In particular, the breakdown of time-temperature superposition can be traced in detail when data covering a broad frequency range are available. We also discuss the temperature dependence of the high-frequency plateau modulus,  $G_{\infty}$ , which can be estimated by means of the PSG. Knowing this quantity is important in some theories and many applications.

### II. EXPERIMENTAL DETAILS

Three different samples of adhesives were studied:

- tesa® 4965 is a commercially available transparent, double-sided tape consisting of a PET backing with a modified acrylic adhesive.
- Sample 09853-08 is a 2-ethylhexyl acrylate polymer (2-EHA + 1%AS) mixture (not commercially available).
- Sample 09853-09 is a mixture of two polymers with quite different glass-transition temperatures,  $T_g$  (not commercially available).

Table I provides an overview of the samples and their glass-transition temperatures,  $T_g$ , measured by differential scanning calorimetry (DSC). All samples were provided by tesa SE and used as received. The optimal sample thickness for the

**TABLE I.** Overview of the different samples, their glass-transition temperatures,  $T_g$  (determined by DSC for a cooling rate of 10 K/min), and the sample thickness. Sample 09853-09 has two glass-transition temperatures because it is a mixture of two polymers. Because the samples are cross-linked and/or blend systems, a quantity like molecular weight is not well-defined.

Sample	$T_g$ (°C)	Thickness (mm)
tesa® 4965	-29	0.21
09853-08	-64	0.24
09853-09	-58/-18	0.25

PSG is around  $250 \,\mu\text{m}$ , which matches the tape® 4965 with a thickness of approximately  $200 \,\mu\text{m}$ . Samples 09853-08 and 09853-09 were made by stacking several sheets of roughly  $50 \,\mu\text{m}$  thickness.

In order to determine the frequency-dependent shear modulus,  $G^*(\omega) = G'(\omega) + iG''(\omega)$ , for a range of temperatures down to  $T_g$ , measurements were performed by the PSG rheometer [26,27], as well as by a standard rheometer.

The original "3PZ-PSG" three-disk version of the PSG [26] was developed to measure the dynamic shear modulus of viscous liquids close to the glass transition. In that version, the disks are electrically coupled so that when the middle disk expands radially, each of the two other disks contracts half as much. We used a new one-disk PSG ("1PZ-PSG") [27] that consists of a single PZ disk with a sample layer on both sides, placed between two solid steel supports that clamp the sample at the contact surface, see Fig. 1. A small hole in the center of the sample layer allows electrical contact to the PZ disk in the middle. Applying an oscillating voltage to the PZ disk induces minute cyclic radial expansions and contractions, which shears the two sample layers sandwiched in-between the disk and the rigid steel supports. The measured capacitance of the PZ disk depends on the strain state of the disk and, thus, on how much the sample resists this deformation. The change in capacitance between the freely moving disk and the disk partially clamped by the sample can be quantitatively translated to the complex shear modulus of the sample (details on the  $\vec{\sigma}$ general modeling can be found in [26] and on the 1PZ-PSG § in [27]). Since it is the deformation of the PZ disk that is measured, the PSG is most sensitive to sample moduli close & to the modulus of the ceramics. This is similar to the compli- $\frac{3}{5}$ ance problem of the standard rheometer, where the instrument itself deforms when the sample gets very stiff, except that in the rheometer case this is an undesired effect that must be corrected for carefully. Christensen and Olsen [26] estimated that the sensitivity range for the PSG is in the  $10^6$ – $10^{10}$  Pa range within a 1% relative error. We, thus, routinely cut off the data points below 1 MPa, which ultimately limits the frequency range in the high-temperature region. The absolute determination of  $G^*$  is also affected by

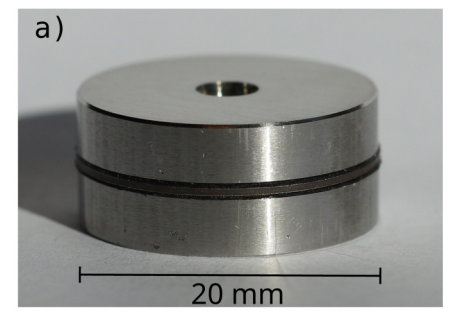




**FIG. 1.** Sample assembly for PSG measurements. (a) "Sandwich" of two outer steel disks around two sample layers with the piezo-ceramic disk in-between. In the case shown, the two sample layers are each of 0.25 mm thickness and the PZ disk 0.5 mm. (b) The assembled PSG with the two steel disks between a frame made of PEEK held together by steel clamps. The large screw at the top ensures electric connection to the piezo-ceramic disk (that has electrodes on both sides).

systematic errors, where the most prominent is the matching of the sample measurement and the reference measurement: the ceramic material of the PZ disk has properties that are temperature dependent *and* depend on the thermal history, and there is a low-frequency dispersion. To obtain accurate results, it is, therefore, necessary to perform two measurements for each thermal protocol: one with sample and one without. Any slight mismatch of the two measurements leads to systematic errors, such as deviations from expected low-frequency power-law behaviors.

All PSG measurements were performed in a custom-built, closed-cycle cryostat [30,31]. The measuring protocol was in all cases to first heat to 315 K, leaving the sample at this elevated temperature for several hours in order to ensure it attaches properly to the disks. After this, the sample was brought to the starting temperature and left there for a sufficient amount of time to equilibrate. Subsequently, samples were measured in temperature steps of 5 K, going down to around  $T_g$ .

The conventional rheometer measurements were carried out on an Anton Paar MCR 702 rheometer in a shear mode with parallel plates. A cyclic strain load amplitude is varied at each measurement frequency, from low amplitude at high frequencies to larger amplitudes at low frequencies. The amplitude range is chosen as a function of the measurement temperature. In the glass range, it starts below 1% at low frequencies and goes down to 0.01% at high frequencies. Only data within the linear viscoelastic range are presented. All samples were of diameter 8 mm, matching the plates, and cut from cross-linked adhesive sheets. The data were compliance corrected, i.e., compensated for the fact that the entire setup is slightly deformed when measuring large modulus samples. The instrument compliance was determined by gluing the upper and lower plate together, measuring at 1 Hz and adjusting the total torsional compliance value until  $\tan \delta$  reached 0.05. The total torsional compliance of the device was determined to have a value of 0.0058 rad/Nm, which was automatically taken into account by the instrument software. When needed, samples were heated to 50 °C with 7.5 °C/min for 5 min to ensure that the adhesive was properly attached to the plates; otherwise, samples were held at 25 °C for 5 min before the cooling was initiated. The samples were cooled to -80 °C at 5 °C/min and subsequently measured during reheating. Measurements started in all cases when the temperature had equilibrated and was stable within  $\pm 0.1$  K. In the temperature range from -80 to 150 °C, a frequency sweep from  $10^{-2}$  to  $10^2$  Hz was performed for all samples in steps of 5 °C. Each frequency sweep took 22 min. At low temperatures, the heating rate was 0.1 °C/min, and at higher temperatures, it was 0.6 °C/min. Dependent on the sample properties, the normal pressure was adjusted from 10 to 0.05 N and adjusted with increasing temperature. By using this procedure, the polymers could follow their thermal expansion.

The expansion coefficient for the samples are around  $6\times 10^{-4}\,\mathrm{K^{-1}}$ , leading to a change in density of around 5% in the temperature range explored here. Both methods take into account the thermal expansion/contraction of the samples.

#### III. RESULTS

This section presents our shear-mechanical data comparing the data from the two techniques.

## A. Consistency between PSG and standard rheometer DMA results

Figure 2 shows the real (left) and imaginary (right) parts of  $G^*(\omega)$  for tesa® 4965 (top), sample 09853-08 (middle), and sample 09853-09 (bottom). The black points give the data obtained by the standard rheometer covering four decades from 0.01 to 100 Hz. The colored points are the PSG data covering from 0.01 Hz to  $\sim$ 20 kHz, i.e., more than six decades. As mentioned, the PSG is not sensitive to low moduli and the data are, thus, cut off below  $\sim$ 1 MPa; this is why the higher-temperature PSG data cover less than six decades. For both methods, spectra were taken at temperatures of 5 K intervals. For clarity, only spectra for every 10 K are shown. The complete data sets for both PSG and rheometer are given in the supplementary material.

Figure 2 demonstrates consistency between the two DMA methods in both temperature dependence and absolute values. The spectra do not line up exactly, because the PSG and rheometer data were not measured at the same temperatures. But even if they were measured at the same nominal temperatures, we would not have a perfect collapse because the absolute temperature calibration in the two measurement setups (of two different laboratories) turned out to not be  $\frac{\overline{\sigma}}{\sigma}$ identical, see Sec. III C. However, the spectra shown for the two methods have the same temperature range. For samples  $\frac{\omega}{N}$ 09853-08 and 09853-09, there is a slight difference in slope of on the low-frequency side at the lowest temperatures, see  $\frac{\omega}{N}$ Figs. 2(c)–2(f). In these cases, the rheological measurements  $\frac{11}{6}$ are more likely to reflect the true dynamics because the PSG data approach the resolution limit of the technique and, thus, are less accurate, while the rheometer is more accurate at these lower moduli at which the instrument compliance affects the measurements less. The reproducibility of these measurements with respect to shape and absolute level is high for both the standard rheology data and the PSG data for the samples 09853-08 and 09853-09. It is somewhat worse for the tesa® 4965 where we find up to a factor 2 difference in absolute levels when comparing the extremes of both techniques; however, the relaxation shape and temperature dependence are recovered by a simple scaling. We speculate that this tape adheres less effectively to the sample cell.

Overall, the data establish that the PSG can be used for extending the frequency range beyond that of standard rheometers for this type of sample. In combination, the two techniques—the rheometer for low frequencies and low moduli, the PSG at high frequencies and high moduli with a significant overlap—constitute a powerful tool to study the full range of the frequency-dependent mechanical dynamics of complex samples.

#### B. Master plots and time-temperature superposition

We proceed to analyze the data as commonly done by constructing master curves. Recall that a master curve gives

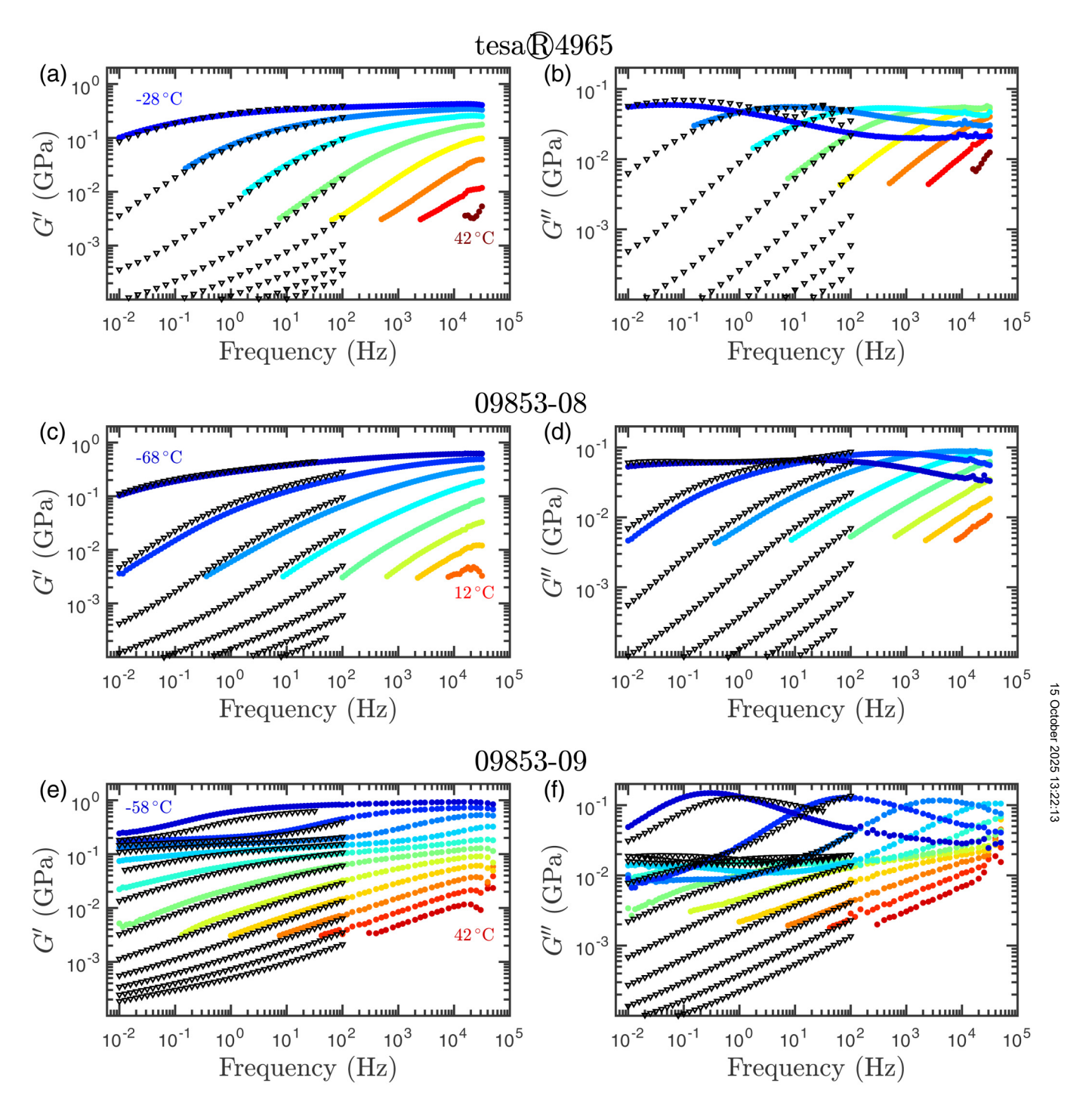


FIG. 2. The logarithm of the real (left column) and imaginary (right column) parts of the shear modulus for (a) and (b) tesa® 4965, (c) and (d) sample 09853-08, and (e) and (f) sample 09853-09. The PSG data are shown as colored circles, the conventional rheometer data as black triangles. The temperature ranges of the PSG/conventional rheometer measurements are as follows: -28 to 42 °C/-30 to 40 °C for tesa® 4965, -68 to 12 °C/-75 to -5 °C for sample 09853-08, and -58 to 42 °C/-53 to 47 °C for sample 09853-09. All spectra were measured in steps of 5 K. For clarity, only spectra for every 10 °C are shown.

the frequency-dependent shear modulus constructed from measurements carried out at different temperatures, the purpose being to determine  $G^*(\omega)$  over a larger frequency range than can be probed by a given technique. The crucial assumption for this to work is time-temperature superposition (TTS), i.e., that different temperatures give rise to identical response functions, merely shifted by a temperature-dependent factor [32–36].

TTS—which is also referred to as thermorheological simplicity, time-temperature scaling, time-temperature

reducibility, or the method of reduced variables [37,38]—amounts to the existence of a (complex) function  $\phi(x)$  such that

$$G^*(\omega, T) = A(T)\phi(\omega\tau(T)). \tag{1}$$

Here, A(T) is an overall scaling factor and  $\tau(T)$  is a characteristic time, the so-called shift factor. In practical applications, the frequency,  $f = \omega/2\pi$ , and a shift factor,  $a_T$ , are

traditionally used instead of  $\omega \tau$ , but the principle is the same. The overall temperature-dependent scaling factor A(T) is not always important; for the construction of the master curves, it can be conveniently scaled out by considering the phase angle  $\delta$  instead of the modulus,

$$\tan \delta = \frac{\sin \delta}{\cos \delta} = \frac{\left|G^*\right| \sin \delta}{\left|G^*\right| \cos \delta} = \frac{\operatorname{Im}(G^*)}{\operatorname{Re}(G^*)} \\
= \frac{\operatorname{Im}(A(T)\phi(\omega\tau(T)))}{\operatorname{Re}(A(T)\phi(\omega\tau(T)))} = \frac{\operatorname{Im}(\phi(\omega\tau(T)))}{\operatorname{Re}(\phi(\omega\tau(T)))} \tag{2}$$

TTS has a history almost as long as the field of rheology itself because if TTS applies, one can determine rheological data over a much wider frequency range than that of the instrument in question. The TTS assumption is a necessity if one used the old-fashioned method of deriving frequencydependent storage and loss moduli from torsion pendulum resonance-frequency experiments, which typically cover less than two decades [33]. A standard rheometer covers four to five decades, as least, but even here TTS is extremely useful if it applies. It has been known for many years, however, that TTS cannot be assumed in general and is, in fact, often violated. This reflects the fact that different relaxation processes are present, in particular in polymers, which usually have different temperature dependencies. There is a very large body of work demonstrating the limitations of TTS. This was undertaken early by Plazek and won him the Bingham medal in 1995, compare his excellent award address [37] reviewing developments that began as early as 1945, a creatively titled paper that with a focus on polyisobutylene data charted the limitations of TTS, especially when there are more than a single type of relaxation. This is relevant, e.g., if there are side groups on the polymer such as PMMA, but Plazek also demonstrated a breakdown of TTS in polystyrene [37]. Despite this well-established knowledge on the limitations of TTS, the TTS assumption is still often used uncritically to create master curves in both academia and industry, the purpose being of course to expand the frequency range of the data.

We constructed master curves of both the standard rheology data and the broadband PSG data presented in Fig. 2 by choosing a reference temperature with a peak in  $\tan \delta$  and then shifting data for other temperatures in frequency to get the best overlap with the reference data. The rheometer and the PSG master curves were constructed separately, but are shown together in Fig. 3 (the two master curves are plotted individually in the supplementary material). Overall, these curves confirm that there is good agreement between the data obtained by the two methods [27]. Figure 3(a) shows the master curves for the sample tape® 4965. For this substance, TTS is obeyed to a good approximation with a single peak of roughly invariant shape of the spectra. The PSG data do, however, reveal that there is a high-frequency secondary process in the kilohertz range. This is not resolved by the rheometer data that display a completely smooth curve. The inset shows the imaginary part of the PSG data, from which it is clear that the secondary process separates out from the primary peak as temperature is lowered. This secondary process is, however, a factor of three to four less intense and does not influence the shape of the primary peak significantly.

For sample 09853-08 in Fig. 3(b), the spectrum is not temperature invariant. On the high-frequency side of the peak, it almost seems as if there are two different curves: a narrow and a very broad one. The inset—again showing the imaginary parts of the PSG data—reveals that this is due to the fact that the single, fairly narrow peak at high temperatures develops a shoulder at low frequencies as temperature is lowered. The shoulder eventually splits into a separate peak of roughly the same intensity. For the PSG data with three to four decades more in frequency (thus having access to both processes at the same temperature), one must decide whether to follow one or the other when constructing the master curve. We used the low-frequency process, leading to the high-frequency part of the curves crossing. The splitting of the spectra into two peaks is also visible in the conventional rheology data, but with a shorter frequency span, this TTS violation is less obvious.

Finally, Fig. 3(c) shows the master curves for sample 09853-09, which is a system of two components with quite different  $T_g$  (see Table I). In this case, two processes are expected to appear in the spectrum: one for component 1 and another for component 2. Because of the different glasstransition temperatures of the two components, one process moves through the frequency window before the second one of appears. For the rheology data, this leads to a master curve a that appears to obey TTS nicely without too much deviation from a single curve shape, including the two peaks corresponding to the two processes. This can be explained by the  $\frac{3}{8}$ limited frequency window in the rheology data, which at no temperature includes both processes and leads to a scaling first of the one process and later of the second. In the PSG data, which access both processes at a range of temperatures, it becomes clear that the temperature dependence of the two are very different. In the inset of Fig. 3(c), two curves at two different temperatures are highlighted with black dashed lines, which shows that at high temperatures, the two processes are closer in frequency, making the low-frequency process a mere shoulder of the more intense high-frequency process, while at low temperatures, the two peaks are clearly separated. The extra frequency range of the PSG method, thus, leads to a quite different master curve than the rheology data in this case.

In Fig. 4, we show the real and imaginary parts of the master curves constructed in Fig. 3 using the same shift factors as in Fig. 3. For all three samples, we still see a decent collapse, but not as good as in Fig. 3. This is because the scaling factor A(T) is eliminated in the master curves in Fig. 3, and the slight misalignment in Fig. 4 could be removed by doing an additional scaling on the y axis. In principle, this would lead to the temperature dependent scaling factor A(T). However, it is important to note here that the order of the scaling is the following: First, one should perform the frequency scaling for  $\tan \delta$  and only then the amplitude scaling on the modulus curves. Doing both on the modulus curves gives too much freedom since, e.g., a

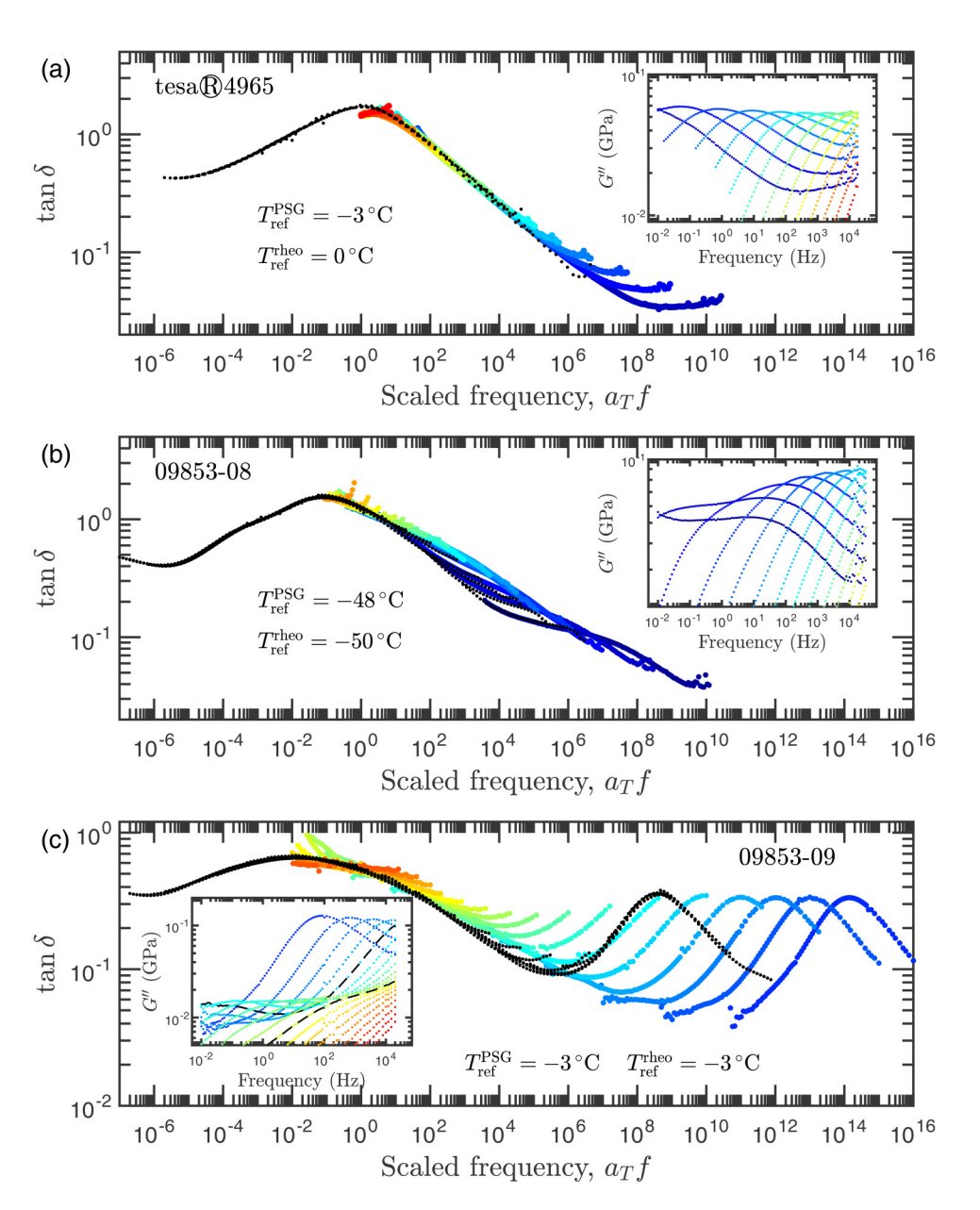


**FIG. 3.** Master curves constructed by shifting  $\tan \delta = G''/G'$  to get optimal overlap. The PSG and rheometer data were constructed separately, but are shown together. Insets show the (unshifted) loss modulus from the PSG data at the temperatures used for the master curves. (a) tesa® 4965, (b) 09853-08, and (c) 09853-09.

power-law curve can be moved arbitrarily. For all three samples, the spectral shape is as expected for cross-linked polymers. At high frequencies, the real part plateaus as the elastic (glassy) region is approached. At low frequencies, neither real nor imaginary part achieve the characteristic limiting power laws of Newtonian flow ( $G' \propto \omega^2$  and  $G'' \propto \omega$ ). Instead, the real and imaginary parts have a much shallower and similar slope typical of cross-linked samples approaching the entanglement plateau.

A standard way to represent data—and to check whether TTS applies—is the van Gurp Palmen plot [39–41]. This plot displays the phase angle  $\delta$  as a function of the modulus  $G^*$  parameterized by the frequency. We show these plots for both methods and the three samples in Fig. 5. To make comparison between the samples easier, we chose to have identical axes on the three plots. Figure 5 confirms the

observations already made that the tesa® 4965 sample obeys TTS to a good approximation while samples 09852-08 and 09853-09 do not. However if one only considers the rheometer data, the conclusion would appear to be that all three samples comply well with TTS, as the rheometer data alone give a good collapse and quite smooth curves. It is only the PSG data with a much broader frequency range that reveal that only the first sample obeys TTS.

What can be learned from Figs. 3–5? The best consistency between the standard rheometer and the PSG master plots is obtained for tesa® 4965, which tells us that TTS is obeyed here to a good approximation. However, even though this is the case, the value of the high-frequency plateau modulus cannot be reliably estimated from the standard rheometer data. Adding the PSG data provides enough extra data at higher frequencies that a loss peak is revealed, above which

15 October 2025 13:22:13

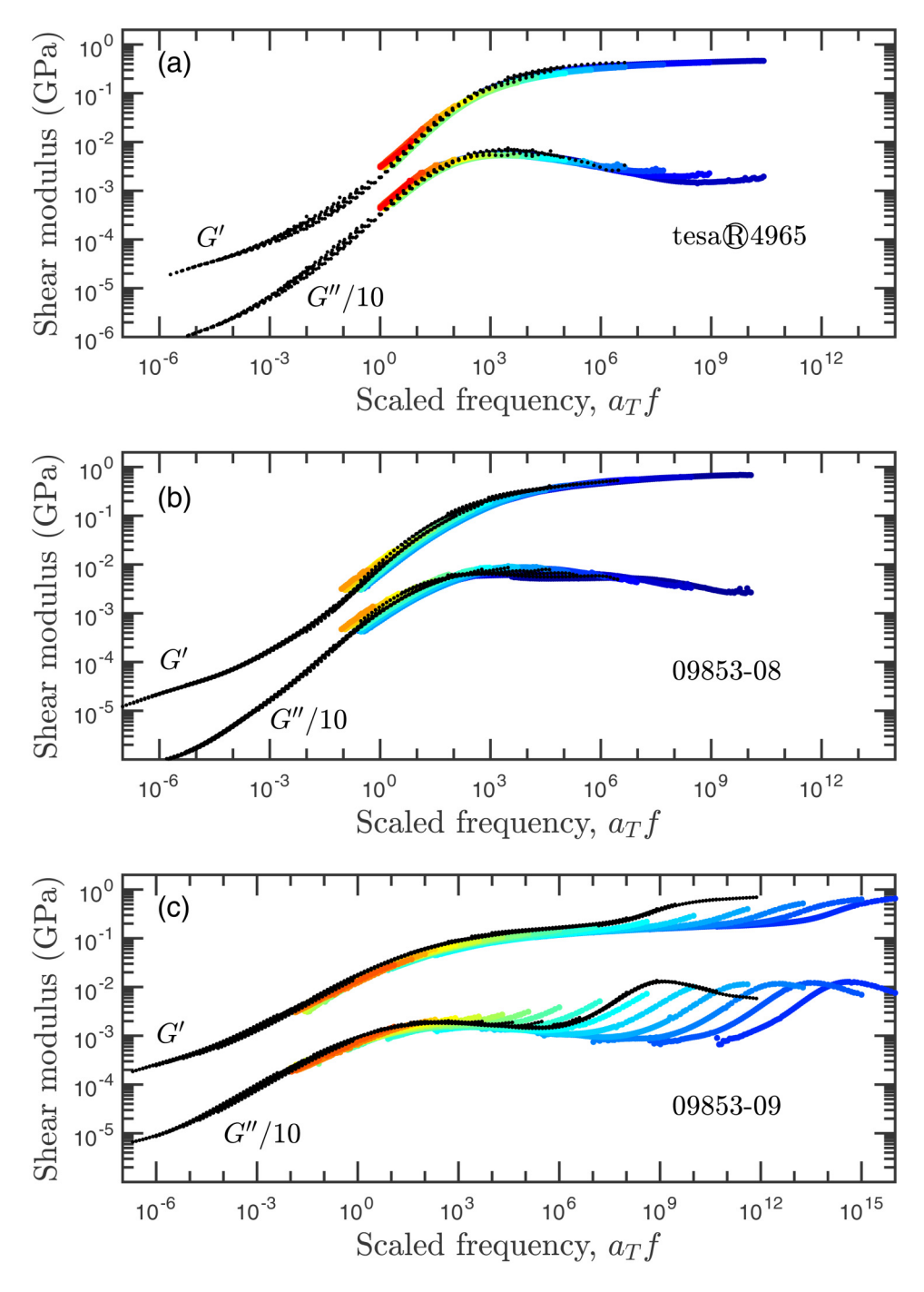


**FIG. 4.** Master curves for G' and G'' using the shifts found in Fig. 3. No shift is made on the y axis, except an overall shift for G'' master curves to separate it from G'. (a) tesa® 4965, (b) 09853-08, and (c) 09853-09.

the modulus levels off and approaches a plateau. In Fig. 5(a), it seems there is a larger spread in the data compared to Fig. 3(a), which appears to be in violation of TTS, but this is due to the lack of scaling on the modulus axis. Recall, there is a temperature dependent scaling factor [A(T) in Eq. (1)] that disappears in  $tan \delta$ , but still influences the data whenever the modulus (be it real, imaginary, or absolute) is plotted. For sample 09853-08, TTS would appear to apply to a very good approximation if only standard rheometer data were available, but the PSG data reveal that TTS does not apply. For sample 09853-09, a similar conclusion applies; in this case, the large difference in temperature dependence of the

first and second peak can be overlooked by the rheometer data with the consequence that the master plot appears deceivingly smooth.

#### C. Temperature dependence of time scales

Figure 6 shows the time scales obtained by the shift factors  $(a_T)$  for the master curves in Fig. 3, as well as the time scales that are visible as peaks in the loss spectrum in the left column for both rheometer and PSG data  $(1/f_{\text{peak}})$ . In the left column [Figs. 6(a), 6(c), and 6(e)], time scales are shown as obtained; clearly, the time scales do not agree

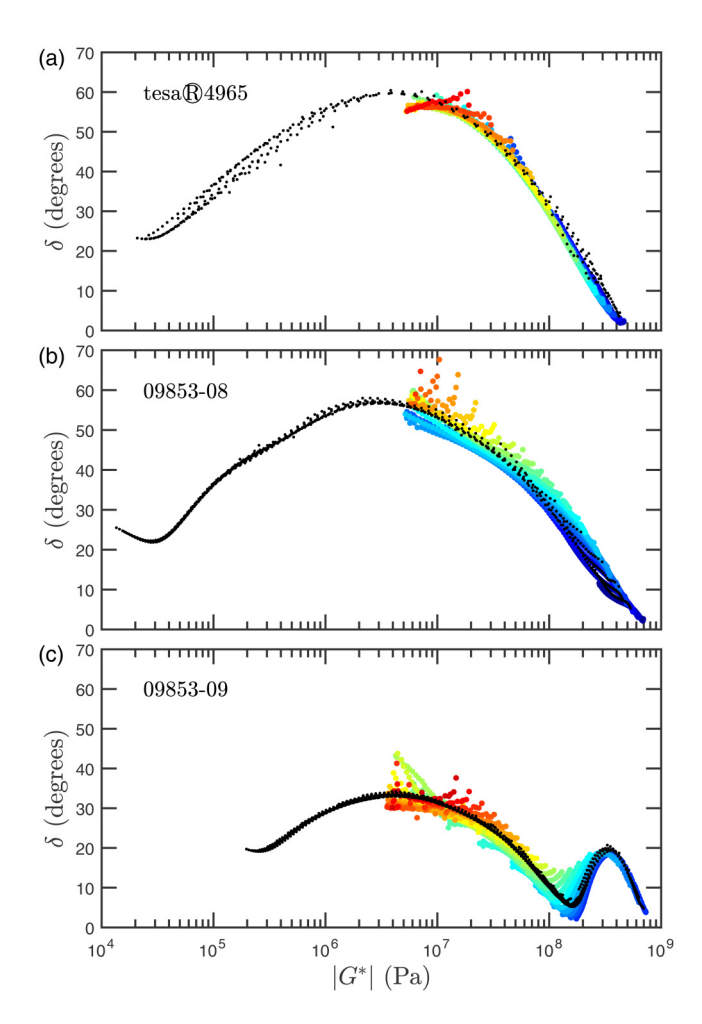


FIG. 5. Parameterized van Gurp Palmen plots for PSG data (colored circles) and rheometer data (black dots) for (a) tesa® 4965, (b) sample 09853-08, and (c) sample 09853-09. A van Gurp Palmen plot [39-41] shows the phase angle  $\delta$  as a function of absolute modulus  $|G^*|$ ; it collapses all curves if the material complies with TTS and the overall scaling A(T) has a negligible temperature dependence.

between shift factors and loss peaks nor between standard rheometer data and PSG data. This is not surprising because (1) the shift factors are on an arbitrary scale determined by the reference temperature (which by definition is a shift factor of 1 s) and (2) the absolute temperature reported for the rheology and PSG setups may not agree. A discrepancy due to either thermal gradients or calibration of some degrees is not uncommon. In order to account for these somewhat arbitrary shifts, we have—in the right column of Fig. 6 brought the shift factors to collapse with the inverse loss peak frequencies at a specific temperature (marked by the vertical dashed line) and subsequently shifted slightly the rheometer data on the temperature axis to give optimal overlap of time scales. The last scaling is to adjust for the difference in absolute temperature calibration between setups. The gray area marks the time scale range of the PSG setup, i.e., where it is, in principle, possible to have direct access to a relaxation time scale. In addition, the glass-transition temperatures from Table I are marked with vertical green dasheddotted lines in all subfigures.

For the tesa® 4965 data in Fig. 6(b), all time scales collapse when scaled and shifted appropriately. This confirms the fact that TTS is obeyed to a good approximation, leaving little ambiguity in the construction of the master curves. In this case, reliable time scales can be derived from the master curve construction. The loss peak time scale corresponding to the glass-transition temperature is between 10 and 100 s, which is not an uncommon correspondence between  $T_g$  as determined by DSC and the kinetic definition of the glass transition.

In Fig. 6(c) (sample 09853-08), the two shift factor curves from the rheometer and the PSG data seem to have quite different temperature dependencies as they cross: the rheometer times are slower than the PSG times at low temperatures but faster at high temperatures. For this sample, the determination of a loss peak frequency was difficult because of the splitting of the peak as mentioned above, and the rheometer data have a visible peak at only one temperature. In Fig. 6(d), it is revealed that when the shift factors for the rheometer and PSG data, respectively, are brought to collapse with the loss peak time scale and subsequently shifted on the temperature axis, the temperature dependence of the shift factors turn out to be identical. On the other hand, the peak-frequency time scales determined from the PSG spectra have a significantly different temperature dependence than that of the shift factors. This most likely reflects the fact that it is very difficult to determine peaks of two processes that close to each other. The loss peak time scale corresponding to the glass-transition temperature for this sample is around  $10^{-2}$  s, which is quite low. This is probably due to the complex spectral shape in this sample splitting of into two relaxation modes at low temperatures [see the inset of § Fig. 3(b)], where the loss peak determined follows the mode at higher frequencies and not the lower-lying modes supposly associated with the glass transition.

For the last sample (09853-09), the picture is even more edly associated with the glass transition.

complicated. In Fig. 6(e), there is a split between the shift factors obtained by rheometer and PSG, respectively, around 250 K. Around the same temperature, there are clearly two different peaks visible in the spectra of both rheometer and PSG data. Above this temperature, there appears to be a collapse of shift factors for the two techniques. But this is deceptive because—as mentioned above—these shift factors are arbitrary and depend on the reference temperature. To be consistent with the above procedures, the shift factors were brought to collapse with the loss peak-frequency time scale at 255 K (marked by a vertical dashed line), and subsequently, the rheometer time scales were shifted on the temperature axis in Fig. 6(f). This scaling does not change the split of time scales, but note that it brings the peak-frequency time scales from both processes and both measurement methods in alignment simultaneously. However, at the same time, it brings the higher temperature time scales out of synchronicity. We interpret this as a sign of the lack of TTS in this sample. If we force the rheometer data to agree with the peak-frequency time scales at 210 K, however, the branch that splits off is completely in sync with the peak frequency of the second process. This confirms that the master curves created based on the rheometer data alone starts out scaling the slowest process and continues to scale the faster process, which clearly leads to an erroneous identification of the time scales. The glass-transition temperatures determined from

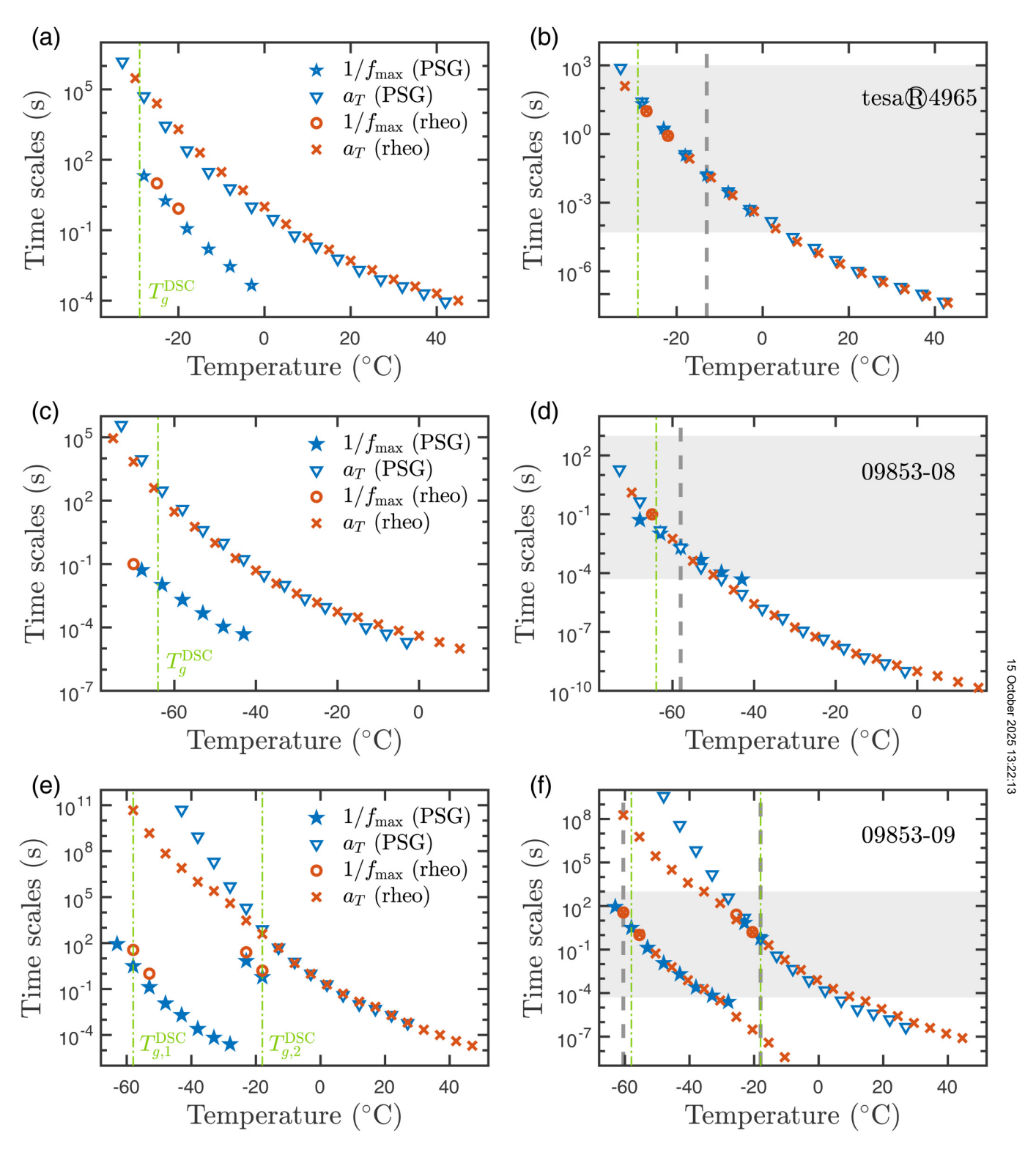


FIG. 6. Time scales obtained as shift factors from the master curve construction (see Fig. 3), as well as the time scales obtained directly from the data as peaks in the loss spectrum. (a), (c), and (e) show time scales as obtained. (b), (d), and (f) show time scales after shift factors have been brought to agree with the loss peak time scales for rheometer and PSG data separately and subsequently shifted on the temperature account for differences in the temperature calibration between setups. Gray shaded areas show the frequency range of the PSG technique. Vertical dashed lines (gray) mark the reference temperature for scaling the PSG shiftfactors to PSG loss peak time scales. Vertical dashed-dotted lines (green) mark the glass-transition temperatures from Table I.

DSC can in this case be used to determine when the master curve for the rheological data follows one process or the other, as the higher one  $(T_{g,2}^{DSC})$  in Fig. 6(e) falls where the shift factors of the standard rheological data split from the shift factors obtained from the PSG data.

# D. Temperature dependence of the high-frequency plateau moduli

An important property of an adhesive is the high-frequency plateau value of the shear modulus,  $G_{\infty}$ , and how this quantity varies with temperature. The "true,"

high-frequency (GHz) plateau cannot be evaluated even from PSG data due to the possible existence of additional highfrequency relaxation processes [15]. Nevertheless, since the PSG goes to much higher frequency than standard rheometers, it makes sense to compare the real and absolute parts of the shear modulus at a fixed (high) frequency for the PSG data, arguing as follows. Figure 7 shows  $G''(10 \,\mathrm{kHz})$  (black open circles) and  $|G^*(10 \text{ kHz})|$  (red triangles) plotted as a function of temperature for all three samples. Where these two curves agree, the imaginary part is much smaller than the real part, meaning that G' has a plateau that tentatively may be interpreted as the true high-frequency plateau modulus,  $G_{\infty}$ . We have highlighted the temperatures at which these two quantities agree to a very good approximation. This applies at low temperatures (note the linear scale used for the modulus, which to some degree hides large relative deviations at the higher temperatures). We conjecture that the highlighted points represent a good estimate of the temperature dependence of  $G_{\infty}$  for each of the samples.

Accepting this interpretation, Fig. 7 demonstrates that for all three samples the plateau modulus is strongly temperature dependent. Indeed, it increases by approximately 50% in the rather narrow temperature range it can be reliably determined. We further note that the samples have quite different plateau values. If TTS applied, one could determine  $G_{\infty}(T)$  within an overall multiplicative constant from the scaling on the y axis in Fig. 4, but this option is not available here.

#### E. Temperature index and the shoving model

A hallmark of glass-forming systems is their dramatic increase in characteristic time scales when cooling of the liquid phase approaching the glass transition [5,33,34,42–44]. In almost all cases, this temperature dependence exceeds that predicted by an Arrhenius equation [45–51] (pure silica is an exception by being almost Arrhenius). This implies that the activation energy for flow is temperature dependent, described by the following equation:

$$\tau(T) = \tau_0 \exp\left\{\frac{\Delta E(T)}{k_B T}\right\},\tag{3}$$

in which  $\tau_0$  is the microscopic time corresponding roughly to the period of a vibration,  $\Delta E(T)$  is the temperature-dependent activation energy (more accurately: free energy of activation), and  $k_B$  is Boltzmann's constant.

An unbiased way of quantifying the temperature dependence of a quantity, X, that increases with decreasing temperature is by the *temperature index* defined as the relative increase in said quantity over the relative decrease in temperature [52],

$$I_X = -\frac{dX/X}{dT/T} = -\frac{d\ln X}{d\ln T}.$$
 (4)

This definition is inspired by the Grüneisen parameter of solid-state physics [53]. If for instance  $I_X = 3$ , this means that lowering the temperature by 1% leads to an increase of X by 3%.

Using  $\Delta E(T) = k_B T \ln{(\tau(T)/\tau_0)}$  and choosing the physically reasonable value  $\tau_0 = 10^{-14} \text{ s}$ , Fig. 8 shows the temperature index of the activation energy as blue triangle-down symbols for all three samples (the large fluctuations reflect the fact that taking a numerical derivative inevitably introduces noise). In all three cases, the temperature index of the activation energy is fairly constant with a value between four and five. Interestingly, these values are similar to those obtained in a study of dielectric relaxation time of 42 simple organic liquids studied close to the glass transition [52].

In the case of sample 09853-09, in addition to the time scales obtained from the shift factors, we also plot the temperature index of the second process (blue stars). Note that the values start a little lower than those of the first process, but increase with decreasing temperature to end at approximately the same level.

The shoving model [42,54] proposes that the abovementioned "super Arrhenius" temperature dependence of the relaxation time (or viscosity) found in nearly all glassforming liquids and polymers and can be accounted for if the activation energy is the energy needed to "shove aside" the surrounding material to create room for a local molecular rearrangement. Such a flow event is so fast that this energy is

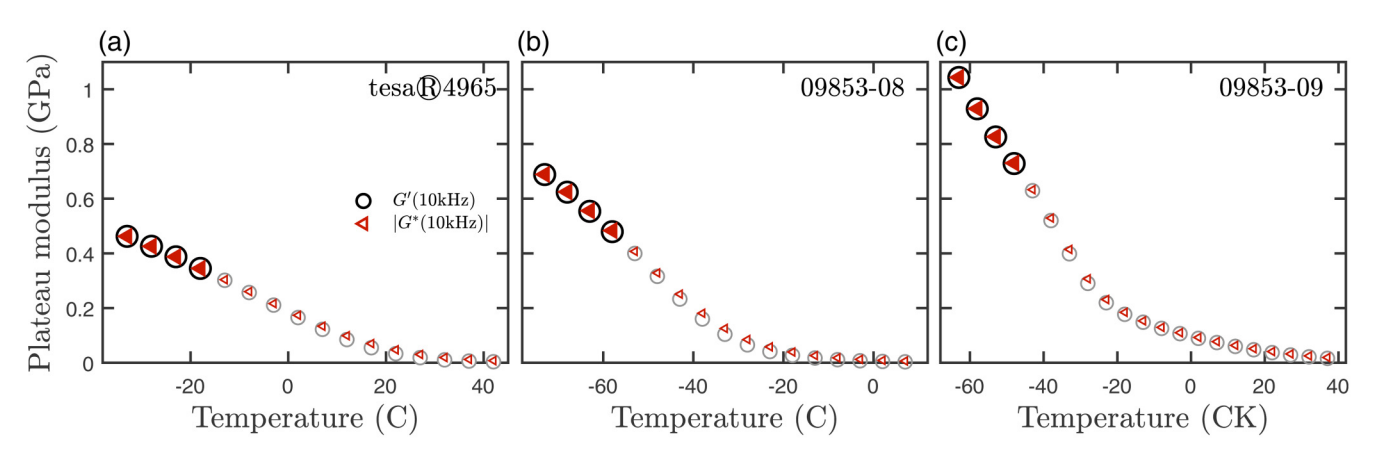
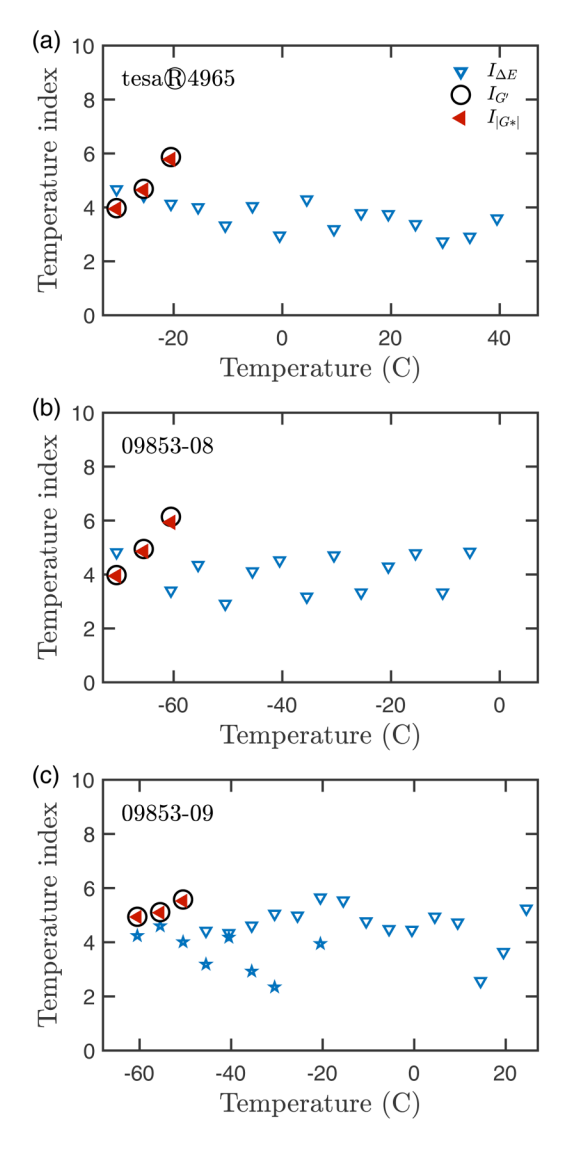


FIG. 7. Temperature dependence of the high-frequency plateau shear modulus,  $G_{\infty}$ , for (a) tesa® 4965, (b) sample 09853-08, and (c) sample 09853-09. Each plot shows the real part, G', and absolute value,  $|G^*|$ , of the PSG data for the highest attainable frequency (between 10 and 50 kHz) as a function of temperature.



**FIG. 8.** Test of the shoving model for (a) tesa® 4965, (b) sample 09853-08, and (c) sample 09853-09. The figure compares the temperature variation of the temperature index (4) of the main relaxation time activation energy (blue triangles) to that of the high-frequency shear modulus' real part (circles) and absolute value (red triangles). The activation-energy temperature index varies little with temperature, whereas that of  $G_{\infty}$  increases upon heating.

of a purely elastic nature; the liquid simply behaves as a solid during the barrier transition [49,55–58]. Since a sphere expanding in an elastic medium makes a pure shear deformation of the surroundings [59], the relevant quantity determining the elastic energy is the high-frequency shear modulus. Thus, the shoving model predicts that

$$\tau(T) = \tau_0 \exp\left\{\frac{V_c G_{\infty}(T)}{k_B T}\right\},\tag{5}$$

where  $V_c$  is a characteristic volume usually assumed to be temperature independent.

The shoving model has been tested on many different glass-forming systems [54,60–63]. It often works well, but not always [63]. To test this model on the present adhesive samples, we added in Fig. 8 the temperature index of the high-frequency plateau modulus found in Sec. III D,

which—if the shoving model applies—is identical to the temperature index of the activation energy. These data points are shown as black open circles and red triangles (same symbols as in Fig. 7). For all three samples, the temperature index of  $G_{\infty}$  increases with temperature, while the temperature index of the activation energy as mentioned has a roughly constant value. However, the  $G_{\infty}$  temperature indices at the lowest temperatures approach the same value.

Interestingly, the trend of an increasing index with increasing temperature goes against what is generally observed for glass-forming liquids [52]. This anomalous temperature variation may indicate that there is still some minor relaxation left at the probed frequency. The agreement between  $I_{G'}$  and  $I_{|G^*|}$  indicates that relaxation has ceased and a true plateau has been reached. In Fig. 8, these quantities are not identical for the higher temperatures, thus showing that some relaxation is still present at that frequency at these temperatures, which will introduce a more severe temperature dependence. At the lowest temperature, the two are practically identical, and, thus, the most reliable  $G_{\infty}$  data are those of the lowest temperature monitored, which is also where the prediction of the shoving model fits data.

#### IV. CONCLUSIONS

Having first demonstrated that there is a high degree of consistency between the PSG and standard rheometer results in the region of overlap for the three studied solid adhesives, this paper has shown that the high-frequency range of the PSG makes it possible to significantly extend the shear-modulus measurements beyond the range of standard rheometers. Our analysis demonstrates that the PSG is well suited for achieving high-quality, reliable rheology results on adhesives. Combined with results measured with a standard rheometer, isothermal shear-modulus curves covering more than six decades in frequency and five decades in modulus were obtained without use of master plots.

We found that the sample tape® 4965 complies with TTS to a good approximation although the PSG data reveal the onset of a high-frequency beta process not resolved by the standard rheometer data. TTS is not obeyed in the two other samples but in those more complex cases, over a limited range, TTS can still yield interesting results if used with caution.

We measured the high-frequency shear-modulus plateau far more accurately than was previously possible and showed that the temperature index of  $G_{\infty}$  at the lowest temperatures, where it is measured most reliably, approaches that of the relaxation time activation energy. This is consistent with the shoving-model prediction.

#### SUPPLEMENTARY MATERIAL

The supplementary material contains all data used in the analysis (only a subset is shown in Fig. 2) with the PSG data and standard rheometer data shown separately for the sake of clarity. In addition, the master curves shown together in Fig. 3 are separated so that they can be inspected individually.

#### **ACKNOWLEDGMENTS**

This work was supported by the VILLUM Foundation's Matter Grant (No. VIL16515).

#### **AUTHOR DECLARATIONS**

#### Conflict of Interest

The authors have no conflicts to disclose.

#### **DATA AVAILABILITY**

The data that support the findings of this study are available from the corresponding author upon reasonable request.

#### **REFERENCES**

- [1] Hopkins, I. L., "Stress relaxation or creep of linear viscoelastic substances under varying temperature," J. Polym. Sci. 28(118), 631-633
- [2] Morland, L. W., and E. H. Lee, "Stress analysis for linear viscoelastic materials with temperature variation," Trans. Soc. Rheol. 4(1), 233-263 (1960).
- [3] Barlow, A. J., A. Erginsav, and J. Lamb, "Viscoelastic relaxation of supercooled liquids," Proc. R. Soc. Lond. 298, 481-494 (1967).
- [4] Lamb, J., "Viscoelasticity and lubrication: A review of liquid properties," J. Rheol. 22, 317-347 (1978).
- [5] Scherer, G. W., Relaxation in Glass and Composites (Wiley, New York, 1986).
- [6] Sollich, P., "Rheological constitutive equation for a model of soft glassy materials," Phys. Rev. E 58, 738-759 (1998).
- [7] Lakes, R. S., "Viscoelastic measurement techniques," Rev. Sci. Instrum. 75(4), 797–810 (2004).
- [8] Bair, S., "Reference liquids for quantitative elastohydrodynamics: Selection and rheological characterization," Tribol. Lett. 22, 197-206
- [9] Doi, M., and S. F. Edwards, The Theory of Polymer Dynamics (Oxford Science Publications, Oxford, 1986).
- [10] Fielding, S. M., P. Sollich, and M. E. Cates, "Aging and rheology in soft materials," J. Rheol. 44(2), 323-369 (2000).
- [11] Adolf, D. B., R. S. Chambers, J. Flemming, J. Budzien, and J. McCoy, "Potential energy clock model: Justification and challenging predictions," J. Rheol. 51, 517-540 (2007).
- [12] Gainaru, C., R. Figuli, T. Hecksher, B. Jakobsen, J. C. Dyre, M. Wilhelm, and R. Böhmer, "Shear-modulus investigations of monohydroxy alcohols: Evidence for a short-chain-polymer rheological response," Phys. Rev. Lett. 112, 098301 (2014).
- [13] Heyes, D. M., D. Dini, and A. C. Branka, "Scaling of Lennard-Jones liquid elastic moduli, viscoelasticity and other properties along fluidsolid coexistence," Phys. Status Solidi B 252, 1514-1525 (2015).
- [14] Klochko, L., J. Baschnagel, J. P. Wittmer, H. Meyer, O. Benzerara, and A. N. Semenov, "Theory of length-scale dependent relaxation moduli and stress fluctuations in glass-forming and viscoelastic liquids," J. Chem. Phys. 156, 164505 (2022).
- [15] Hecksher, T., D. H. Torchinsky, C. Klieber, J. A. Johnson, J. C. Dyre, and K. A. Nelson, "Toward broadband mechanical spectroscopy," Proc. Natl. Acad. Sci. U. S. A. 114, 8710-8715 (2017).
- [16] Willenbacher, N., and C. Oelschlaeger, "Dynamics and structure of complex fluids from high frequency mechanical and optical rheometry," Curr. Opin. Colloid Interface Sci. 12(1), 43-49 (2007).

- [17] Schroyen, B., D. Vlassopoulos, P. Van Puyvelde, and J. Vermant, "Bulk rheometry at high frequencies: A review of experimental approaches," Rheol. Acta 59, 1-22 (2020).
- [18] Neshasteh, H., I. Shlesinger, M. Ravaro, M. Gely, G. Jourdan, S. Hentz, and I. Favero, "Optomechanical micro-rheology of complex fluids at ultra-high frequency," Nat. Commun. 16, 407 (2025).
- [19] Yan, Y.-X., and K. A. Nelson, "Impulsive stimulated light scattering. II. Comparison to frequency-domain light-scattering spectroscopy," J. Chem. Phys. 87(11), 6257–6265 (1987).
- [20] Klieber, C., T. Pezeril, S. Andrieu, and K. A. Nelson, "Optical generation and detection of gigahertz-frequency longitudinal and shear acoustic waves in liquids: Theory and experiment," J. Appl. Phys. 112, 013502 (2012).
- [21] Pezeril, T., C. Klieber, S. Andrieu, and K. A. Nelson, "Optical generation of gigahertz-frequency shear acoustic waves in liquid glycerol," Phys. Rev. Lett. 102, 107402 (2009).
- [22] Pottier, B., A. Raudsepp, C. Frétigny, F. Lequeux, J.-F. Palierne, and L. Talini, "High frequency linear rheology of complex fluids measured from their surface thermal fluctuations," J. Rheol. 57, 441–455 (2013).
- [23] Pine, D. J., D. A. Weitz, P. M. Chaikin, and E. Herbolzheimer, "Diffusing wave spectroscopy," Phys. Rev. Lett. 60, 1134-1137 (1988).
- [24] Kőkuti, Z., K. van Gruijthuijsen, M. Jenei, G. Tóth-Molnár, A. Czirják, J. Kokavecz, P. Ailer, L. Palkovics, A. C. Völker, and G. Szabó, "High-frequency rheology of a high viscosity silicone oil using diffusing wave spectroscopy," Appl. Rheol. 24(6), 63984 (2014).
- [25] Athanasiou, T., G. K. Auernhammer, D. Vlassopoulos, and G. Petekidis, "A high-frequency piezoelectric rheometer with validation of the loss angle measuring loop: Application to polymer melts 9 and colloidal glasses," Rheol. Acta 58, 619-639 (2019).
- [26] Christensen, T., and N. B. Olsen, "A rheometer for the measurement & of a high shear modulus covering more than seven decades of frequency below 50 kHz," Rev. Sci. Instrum. 66(10), 5019–5031 (1995).
- [27] Mikkelsen, M., K. L. Eliasen, N. Lindemann, K. Moch, R. Böhmer, a H. A. Karimi-Varzaneh, J. Lacayo-Pineda, B. Jakobsen, K. Niss, T. Christensen, and T. Hecksher, "Piezo-electric shear rheometry: Further developments in experimental implementation and data extraction," J. Rheol. 66(5), 983-1003 (2022).
- [28] Chen, C. P., and R. S. Lakes, "Apparatus for determining the viscoelastic properties of materials over ten decades of frequency and time," J. Rheol. 33, 1231-1249 (1989).
- [29] Koganezawa, S., Y. Katsuta, R. Lu, H. Tani, and N. Tagawa, "Device for direct measurement of dynamic viscoelastic properties of solid-state materials at frequencies higher than 1 kHz," Rheol. Acta 56, 477-486 (2017).
- [30] Igarashi, B., T. Christensen, E. H. Larsen, N. B. Olsen, I. H. Pedersen, T. Rasmussen, and J. C. Dyre, "A cryostat and temperature control system optimized for measuring relaxations of glass-forming liquids," Rev. Sci. Instrum. 79, 045105 (2008).
- [31] Igarashi, B., T. Christensen, E. H. Larsen, N. B. Olsen, I. H. Pedersen, T. Rasmussen, and J. C. Dyre, "An impedance-measurement setup optimized for measuring relaxations of glass-forming liquids," Rev. Sci. Instrum. 79, 045106 (2008).
- [32] Ferry, J. D., Viscoelastic Properties of Polymers, 2nd ed. (Wiley, New York, 1970).
- [33] Harrison, G., The Dynamic Properties of Supercooled Liquids (Academic, New York, 1976).
- [34] Angell, C. A., K. L. Ngai, G. B. McKenna, P. F. McMillan, and S. W. Martin, "Relaxation in glassforming liquids and amorphous solids," J. Appl. Phys. 88, 3113-3157 (2000).

- [35] Olsen, N. B., T. Christensen, and J. C. Dyre, "Time-temperature superposition in viscous liquids," Phys. Rev. Lett. 86, 1271-1274 (2001).
- [36] Götze, W., Complex Dynamics of Glass-Forming Liquids: A Mode-Coupling Theory (Oxford University, New York, 2009).
- [37] Plazek, D. J., "1995 Bingham Medal Address: Oh, thermorheological simplicity, wherefore art thou?" J. Rheol. 40, 987-1014 (1996).
- [38] Blochowicz, Th., Ch. Tschirwitz, St. Benkhof, and E. A. Rössler, "Susceptibility functions for slow relaxation processes in supercooled liquids and the search for universal relaxation patterns," J. Chem. Phys. 118(16), 7544-7555 (2003).
- [39] van Gurp, M., and J. Palmen, Time-temperature superposition for polymeric blends, in Proceedings XIITH International Congress on Rheology, Qiuebec City, Canada, August 18-23, 1996 edited by A. AitKadi, J. Dealy, D. James, and M. Williams (The Society of Rheology, 1996), pp. 134-135.
- [40] Trinkle, S., and C. Friedrich, "Van Gurp-Palmen-plot: A way to characterize polydispersity of linear polymers," Rheol. Acta 40, 322-328
- [41] Qian, Z., and G. B. McKenna, "Expanding the application of the van Gurp-Palmen plot: New insights into polymer melt rheology," Polymer **155**, 208–217 (2018).
- [42] Dyre, J. C., "The glass transition and elastic models of glass-forming liquids," Rev. Mod. Phys. 78, 953-972 (2006).
- [43] Berthier, L., and G. Biroli, "Theoretical perspective on the glass transition and amorphous materials," Rev. Mod. Phys. 83, 587-645 (2011).
- [44] Mauro, J. C., Materials Kinetics: Transport and Rate Phenomena (Elsevier, Amsterdan, 2021).
- [45] Angell, C. A., "Formation of glasses from liquids and biopolymers," Science 267, 1924-1935 (1995).
- [46] Ediger, M. D., C. A. Angell, and S. R. Nagel, "Supercooled liquids and glasses," J. Phys. Chem. 100, 13200-13212 (1996).
- [47] Debenedetti, P. G., and F. H. Stillinger, "Supercooled liquids and the glass transition," Nature 410, 259-267 (2001).
- [48] Hunter, G. L., and E. R. Weeks, "The physics of the colloidal glass transition," Rep. Prog. Phys. 75, 066501 (2012).
- [49] Wang, W. H., "The elastic properties, elastic models and elastic perspectives of metallic glasses," Prog. Mater. Sci. 57, 487-656 (2012).

- [50] McKenna, G. B., and S. L. Simon, "50th anniversary perspective: Challenges in the dynamics and kinetics of glass-forming polymers," Macromolecules 50, 6333-6361 (2017).
- [51] Alba-Simionesco, C., and G. Tarjus, "A perspective on the fragility of glass-forming liquids," J. Non-Cryst. Solids X 14, 100100 (2022).
- [52] Hecksher, T., A. I. Nielsen, N. B. Olsen, and J. C. Dyre, "Little evidence for dynamic divergences in ultraviscous molecular liquids," Nat. Phys. 4, 737-741 (2008).
- [53] Ashcroft, N. W., and N. D. Mermin, Solid State Physics (Holt, Rinehart and Winston, London, 1976).
- [54] Dyre, J. C., N. B. Olsen, and T. Christensen, "Local elastic expansion model for viscous-flow activation energies of glass-forming molecular liquids," Phys. Rev. B 53, 2171–2174 (1996).
- Mooney, M., "A theory of the viscosity of a Maxwellian elastic liquid," Trans. Soc. Rheol. 1, 63-94 (1957).
- [56] Dyre, J. C., "Source of non-Arrhenius average relaxation time in glassforming liquids," J. Non-Cryst. Solids 235-237, 142-149 (1998).
- [57] Khonik, V. A., Yu. P. Mitrofanov, S. A. Lyakhov, D. A. Khoviv, and R. A. Konchakov, "Recovery of structural relaxation in aged metallic glass as determined by high-precision in situ shear modulus measurements," J. Appl. Phys. 105, 123521 (2009).
- [58] Dyre, J. C., "Solid-that-flows picture of glass-forming liquids," J. Phys. Chem. Lett. 15, 1603-1617 (2024).
- [59] Landau, L. D., and E. M. Lifshitz, Theory of Elasticity (Elsevier, New York, 1986).
- [60] Niss, K., B. Jakobsen, and N. B. Olsen, "Dielectric and shear mechanical relaxations in glass-forming liquids: A test of the Gemant-DiMarzio-Bishop model," J. Chem. Phys. 123, 234510
- [61] Torchinsky, D. H., J. A. Johnson, and K. A. Nelson, "A direct test of S the correlation between elastic parameters and fragility of ten glass formers and their relationship to elastic models of the glass transition," J. Chem. Phys. 130, 064502 (2009).
- [62] Dyre, J. C., and W. H. Wang, "The instantaneous shear modulus in the N shoving model," J. Chem. Phys. 136, 224108 (2012).
- [63] Hecksher, T., and J. C. Dyre, "A review of experiments testing the shoving model," J. Non-Cryst. Solids 407, 14-22 (2015).